J. Adhesion Sci. Technol., Vol. 17, No. 8, pp. 1055–1073 (2003)

Also available online - www.vsppub.com

Synthetic gecko foot-hair micro/nano-structures as dry adhesives

METIN SITTI [1,*] and RONALD S. FEARING [2]

[1] *Department of Mechanical Engineering and The Robotics Institute, Carnegie Mellon University, Pittsburgh, PA 15213-3890, USA*
[2] *Department of Electrical Engineering and Computer Sciences, University of California at Berkeley, Berkeley, CA 94720-1770, USA*

Received in final form 7 March 2003

Abstract—This paper proposes techniques to fabricate synthetic gecko foot-hairs as dry adhesives for future wall-climbing and surgical robots, and models for understanding the synthetic hair design issues. Two nanomolding fabrication techniques are proposed: the first method uses nanoprobe indented flat wax surface and the second one uses a nano-pore membrane as a template. These templates are molded with silicone rubber, polyimide, etc. type of polymers under vacuum. Next, design parameters such as length, diameter, stiffness, density, and orientation of hairs are determined for non-matting and rough surface adaptability. Preliminary micro/nano-hair prototypes showed adhesion close to the predicted values for natural specimens (around 100 nN each).

Keywords: Biomimetic adhesives; pressure controlled dry adhesives; adhesion forces; polymer micro/nano-fabrication; micro/nano-robotics; nanoindentation; and nanomolding.

1. INTRODUCTION

Nanotechnology is one of the key technologies of this century for novel information technology and biotechnology products. On the other hand, nanotechnology would enable novel materials for robotics applications, and this paper is focused on developing biologically inspired dry adhesives using nanofabrication techniques for future wall-climbing and surgical robots and also other general dry adhesive applications. Geckos can climb and run on wet or dry and molecularly smooth or very rough surfaces with very high maneuverability and efficiency. To get similar performance from wall-climbing robots, foot sticking and releasing mechanism is the critical component. Geckos have compliant micro- and nanoscale high aspect

*To whom correspondence should be addressed. Phone: (412) 268 3632. Fax: (412) 268 3348. E-mail: msitti@andrew.cmu.edu

ratio beta-keratin structures at their feet to adhere to any surface with a pressure controlled contact area [1]. This adhesion is mainly due to the molecular forces such as van der Waals forces [2].

The hierarchical structure of the *Tokay* gecko foot-hair is shown in Fig. 1. Scanning electron microscope (SEM) is used for sub-micrometer and nanometer resolution images in the figure. Foot-hairs start from the micrometer scale (stalks) and go down to 100–200 nm diameter (spatular stalks) by branching [1]. Also, there are oriented caps (spatulae) with about 300–500 nm width at the very ends of spatular stalks. This paper is focused on fabricating synthetic gecko foot-hair spatular stalks (nano-hairs) and setal stalks (micro-hairs). 3D fabrication of spatulae is a future work.

The basic features of the synthetic hair fabrication can be given as follows: (1) High aspect ratio micrometer (1 : 10–30) and nanometer (1 : 20–50) scale structure fabrication with diameters of 3–10 μm and 50–500 nm, respectively, (2) Maximize micro/nano-hair density (number of hairs in a given area, e.g. 1 cm^2) for higher adhesion, (3) Maximize nano-hair stiffness to prevent matting, and (4) Material properties of synthetic hairs: Young's modulus of 1–15 GPa, hydrophobic, and high tensile strength.

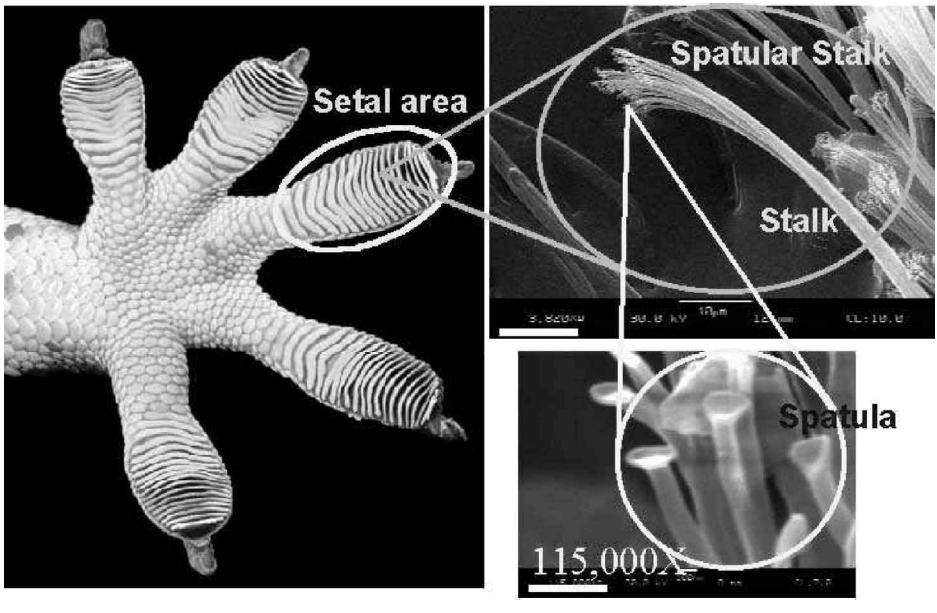

Figure 1. *Tokay* gecko foot-hair images: gecko foot bottom view (left image); zooming into one of the stalks under SEM (right upper image, bar indicates 10 μm), and zooming into spatulae and spatular stalks at the end of a stalk under SEM (right lower image, bar indicates 300 nm) (courtesy of Kellar Autumn).

2. FABRICATION METHODS

To fabricate synthetic hairs with the above features, a master template that has micrometer- or nanometer-scale high aspect ratio holes representing the negative of the synthetic hairs is molded with liquid polymers [3, 4]. Then the molded polymer is cured and separated from the template by peeling off or etching. Two different methods using this nanomolding technique are explained below.

2.1. Method I: nanorobotic imprinting

For this first method, the shape of a fabricated nanostructure, e.g. (1) a nanotip such as an atomic force microscope (AFM) or a scanning tunnelling microscope probe tip, a glass pipette, etc. (2) array of these nanotips, or (3) any other high aspect ratio micro/nano-structure array, is imprinted on a flat soft surface by indenting. Previously, nanotip arrays were used as templates for imprint patterning of a polystyrene surface with 0.8 μm diameter and 3 μm depth holes [5]. Also, PMMA [poly(methyl methacrylate)] was indented by an AFM probe for data-storage applications [6] or by a tip array and molded with a metal layer for patterning down to 40 nm metallic contacts [7].

In this paper, a single AFM probe (Nanosensors Inc., Neuchatel, Switzerland, 42 N/m stiffness, conical tip of apex radius 10–20 nm, and 15 μm height) is used to indent a flat wax surface (J. Freeman Inc., Dorchester, MA) as can be seen in Fig. 2. By indenting the wax surface, the template as given in Fig. 3a was obtained. The profile of the indented wax surface can be seen in Fig. 3b. After molding with silicone rubber or any other polymer and separating the polymer from the wax template by peeling, synthetic nano-bumps of Fig. 3c were obtained. This process could be repeated autonomously to fabricate a large number of nano-bumps, and even oriented hairs can be fabricated by tilting the wax surface during indentation and using closed-loop force-feedback control. An array of rubber nano-bumps made by manual step-and-repeat indenting is displayed in Fig. 4.

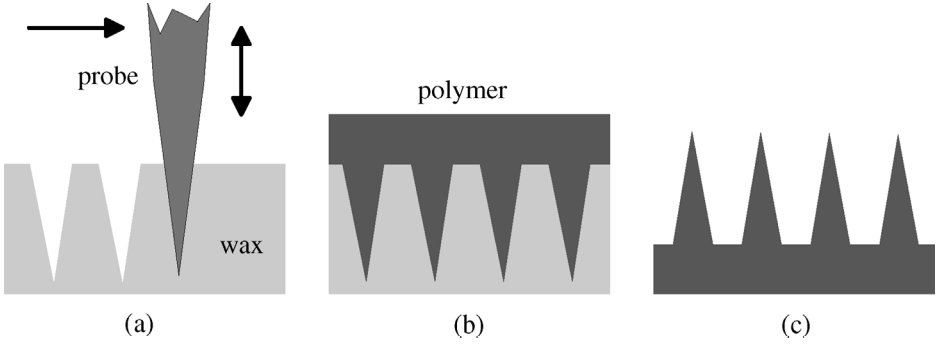

Figure 2. Synthetic hair fabrication by the Method I: (a) Indenting a flat wax surface using a micro/nano-fabricated probe nanotip, (b) molding it with a polymer, and (c) separating the polymer from the wax by peeling.

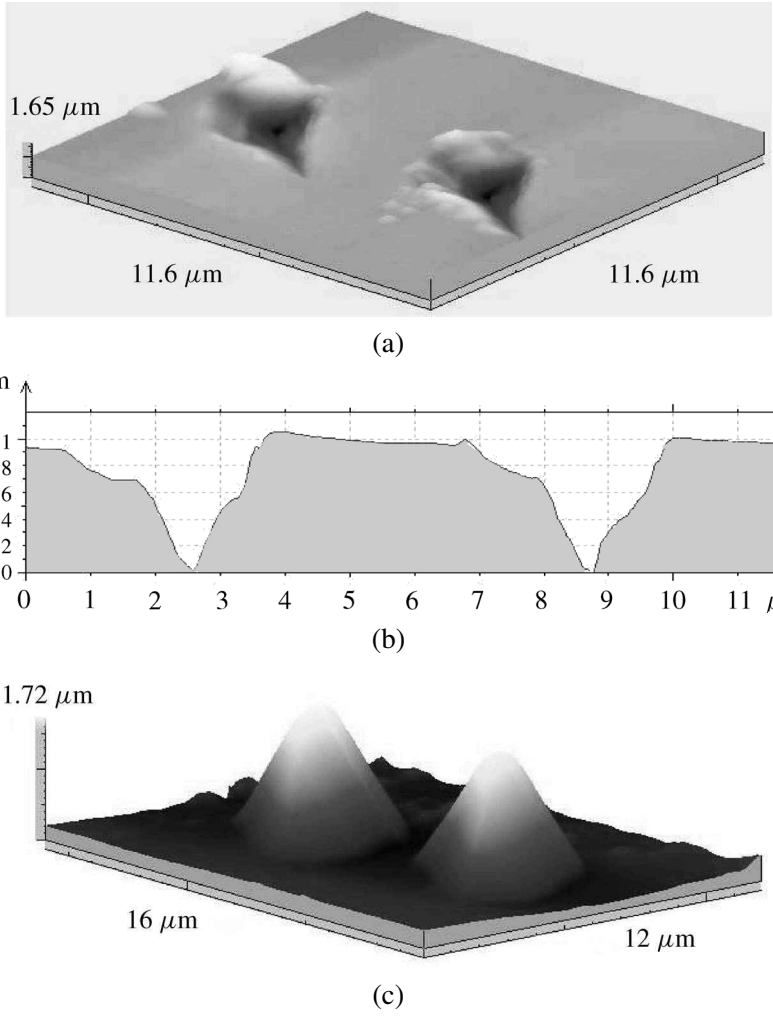

Figure 3. 3D AFM tapping mode image of (a) the flat wax surface ($11.5 \times 11.6 \times 1.65\ \mu m^3$ image size) indented by an AFM probe nanotip, (b) profile of the indented wax surface, and (c) molded and peeled off silicone rubber nano-bumps ($16 \times 12 \times 1.7\ \mu m^3$ image size).

Synthetic nano-bumps were fabricated from two different hydrophobic polymer materials (around 87° contact angle with deionized water): silicone rubber (Dow Corning Inc., HS II, Midland, MI) and polyester resin (TAP Plastics Inc., Stockton, CA). Silicone rubber Young's modulus was measured as 0.57 MPa. It was determined by measuring the stiffness of a molded known-size rectangular rubber beam. However, feather beta-keratin has the elastic modulus of 1–10 GPa [8], and gecko foot-hairs are estimated in the range of 1–15 GPa from our measurements using an AFM probe based bending of a single *Tokay* gecko stalk. While rubber has good adhesion properties, we had some concern that the natural stickiness of rubber might be contributing the measured adhesion force, rather than a more universal

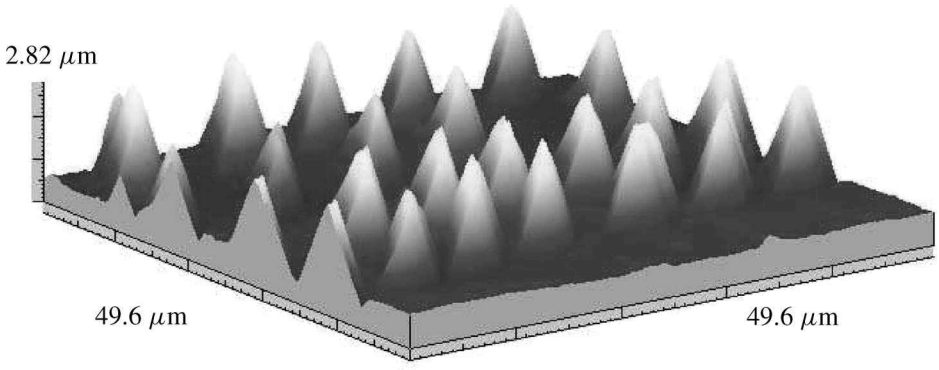

Figure 4. 3D AFM tapping mode image of a silicone rubber nano-bump array fabricated by step-and-repeat based AFM probe nanotip indenting.

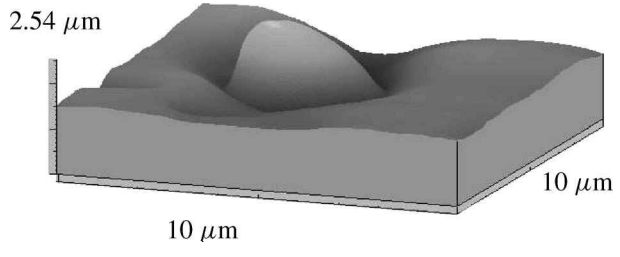

Figure 5. A polyester synthetic nano-bump fabricated by molding a wax surface indented by an AFM probe nanotip.

van der Waals attraction. Thus, polyester was also tried as the molding polymer material. Polyester Young's modulus is measured as around 0.85 GPa. Thus, it is a better match to the natural nano-hair modulus. A molded polyester bump is shown in Fig. 5.

To characterize the adhesion of synthetic hairs to a silicon surface with a natural oxide layer, pull-off force measurements were conducted using unloading force-distance plots as in Fig. 6 with an AFM (Metrology AFM, Molecular Imaging Inc., Tempe, AZ) and a tipless rectangular silicon AFM probe with 1.75 N/m stiffness and 390 nm/s retraction speed. In the unloading force-distance curves, the maximum attractive (pull-off) force gives the adhesion of the synthetic nano-bump to the probe SiO_2 surface. Measurements were made in a laboratory environment with 25°C and 58% relative humidity. Pull-off force was measured as 181 ± 9 nN (25 samples) for silicone rubber nano-bumps with tip radius range of 230–440 nm (measured from the 3D AFM image) and 294 ± 21 nN (20 samples) for polyester nano-bump with tip radius of 350 nm. We thus have shown good reproducibility. The root-mean-square surface roughnesses of silicone rubber and polyester flat substrates were measured by AFM as ≈3 nm and ≈5 nm, respectively. Since these values are relatively small and we could not measure the roughness at the tip of the synthetic nano-bumps directly, the roughness effect on surface forces was neglected.

Pull-off force between a spherical tip and flat surface is given by the Johnson–Kendall–Roberts (JKR) theory as $F = 1.5\pi R W_{12}$, where $W_{12} = \gamma_1 + \gamma_2 - \gamma_{12} \approx 2\sqrt{\gamma_1 \gamma_2}$ [9] is the work of adhesion, γ_{12} is the interfacial energy, and R is the spherical tip radius. $\gamma_1 = 160 \pm 40$ mJ/m^2 [10] and γ_2 are the surface energies of the SiO_2 layer and the polymer, respectively. For silicone rubber with $\gamma_2 = 21.4$ mJ/m^2 [12], 185 nN pull-off force is theoretically expected taking $R \approx 335$ nm. For polyester with $\gamma_2 = 44.6$ mJ/m^2 [12], 279 nN is expected. These expected adhesion forces are very close to the measured ones.

This adhesion force is consistent with van der Waals force. For calculating the van der Waals contribution to these adhesion forces, $F_{vdW} = HR/6d_0^2$ is used where $d_0 \approx 0.165$ nm is the approximate interfacial cut-off distance [9] and H is the Hamaker constant. Using $H \approx 45 \times 10^{-21}$ J (estimated from $H = 2.1 \times 10^{-18}\gamma$ [9] where γ is the surface energy in J/m^2 units) for rubber, $H = 60.5 \times 10^{-21}$ J [11] for polyester, and $H = 68.5 \times 10^{-21}$ J [11] for SiO_2, and $F_{vdW} = 114$ nN and $F_{vdW} = 139$ nN are predicted for silicone rubber and polyester, respectively. Thus, 47–63% of the adhesion forces of the synthetic nano-bumps are due to the van der Waals forces while the rest could be due to polar interactions, other adhesion effects, and surface roughness effects.

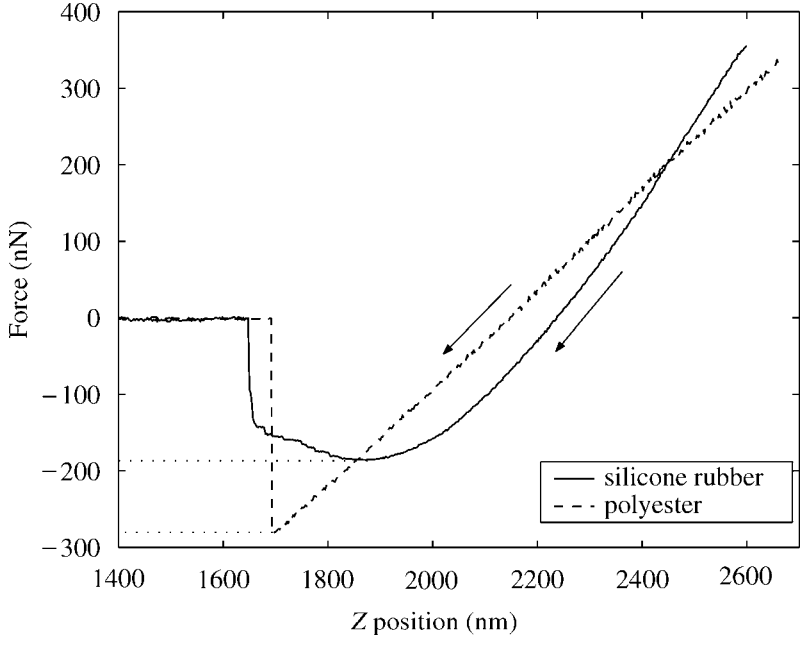

Figure 6. Pull-off force measurements on the synthetic (silicone rubber (solid line) and polyester (dashed line)) nano-bumps using a tipless AFM probe (arrows indicate the unloading direction).

Table 1.
Properties of nano-pore membranes

Material	Pore size (μm)	Thickness (μm)	Pore density (pores/cm^2)
Alumina	0.02–0.2	60	10^9
Polycarbonate	0.02–20	7–14	10^5–10^8

2.2. Method II: parallel fabrication

For this second fabrication method, a membrane with self-organized high aspect ratio pores was used as the master template and molded with a liquid polymer. Two types of membranes were used: alumina (Nanopore, Whatman Inc., Clifton, NJ) and polycarbonate (Poretics, Osmonics' Lab Inc., Minnetonka, MN) membranes. They have different ranges of diameter, density and thickness of micro/nano-pores, Young's modulus, maximum possible temperature before plastically deforming, etching properties, etc. (Table 1).

First, an alumina membrane (Fig. 7a) with 200 nm diameter and 60 μm thick perpendicular nanopores was molded with silicone rubber as shown in Fig. 7b under vacuum. As can be seen from the figure, 60 μm long nano-hairs are too compliant and too dense (i.e. too close to each other) to prevent self-sticking. However, this result demonstrates the feasibility of molding nanopores with 200 nm pore sizes with liquid polymers under vacuum where at these small scales it gets very challenging to flow liquid polymers through pores due to increased surface and drag forces.

For shortening the nano-hairs and decreasing the nano-hair density, polycarbonate membranes were used. These membranes have a random orientation of the nano-pores ($\pm 15^\circ$) created by a nuclear track etch. The SEM micrograph of the polycarbonate membrane is displayed in Fig. 8a. A 8 μm diameter polycarbonate membrane was molded with silicone rubber under vacuum and the rubber was peeled off from the membrane after curing at room temperature for 24 h. Resulting rubber hairs with about 6 μm diameter and length are shown in Fig. 8b. Smaller diameter (down to 100 nm) membrane molding is currently in progress. Adhesion of rubber hair array in Fig. 8b to a flat glass substrate was measured using a force sensor of about 2.8 mN/cm^2 for a 25 mN preload. This implies about 60 nN adhesion for each single hair using the fabricated hair density of 5×10^4 pores/cm^2 and assuming all hairs contact the substrate.

3. GECKO SPATULA HAIR MODEL

To understand the effect of nano-hair size, density and orientation, a spatular hair is modelled as a simple cantilever beam. By proper choice of hair length, angle, density and diameter, hairs can stick to very rough surfaces. To avoid hairs tangling,

they need to be sufficiently stiff and separated while still dense enough to provide enough adhesion force.

An array of bumps, even with a compliant backing, will have difficulty adhering to a non-smooth surface as shown in Fig. 9a. In fact, it is reasonable to assume that two rigid non-smooth planar surfaces will contact at only 3 points, hence the adhesion of an array of nano-bumps will be quite minimal. Each spatula must be able to adapt to surface height variations as shown in Fig. 9b. This is necessary condition #1: *Rough Surface Compatibility*. By making the hairs very high aspect ratio and skinny, they can adapt and adhere to rough surfaces when they are pressed against the surface. The problem with high aspect ratio and skinny hairs is that the

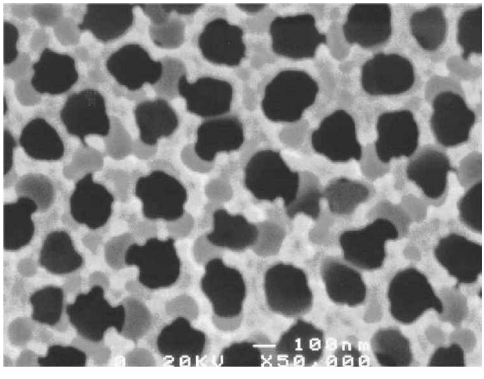

(a)

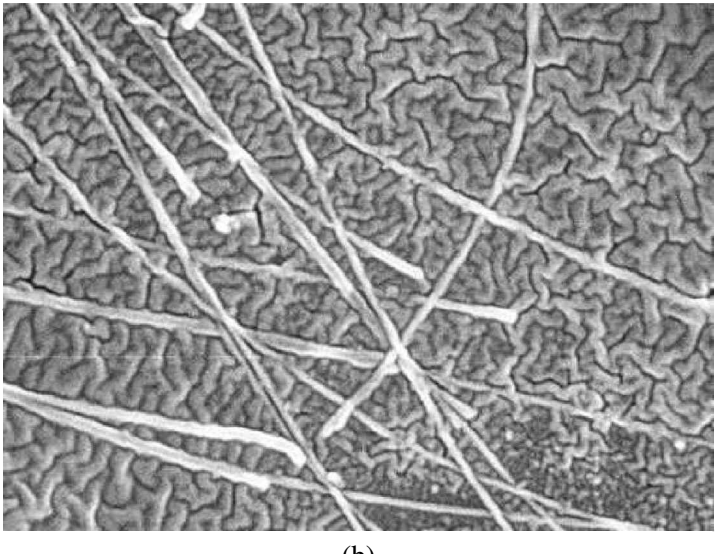

(b)

Figure 7. Top-view SEM images of (a) alumina membrane with 200 nm diameter pores, (b) molded silicone rubber nano-hairs with 200 nm diameter, 60 μm total length, and about 100 nm spacing between hair bases (rubber nano-hairs are laying on a flat rubber surface).

hairs are as likely to stick to each other as to the substrate, becoming hopelessly matted and tangled, (Necessary condition #2: *Non-Matting Constraints*). A third condition, which is desirable, is that the hairs be self-cleaning. The self-cleaning condition is future work.

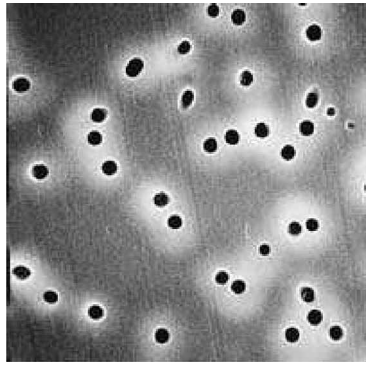

(a)

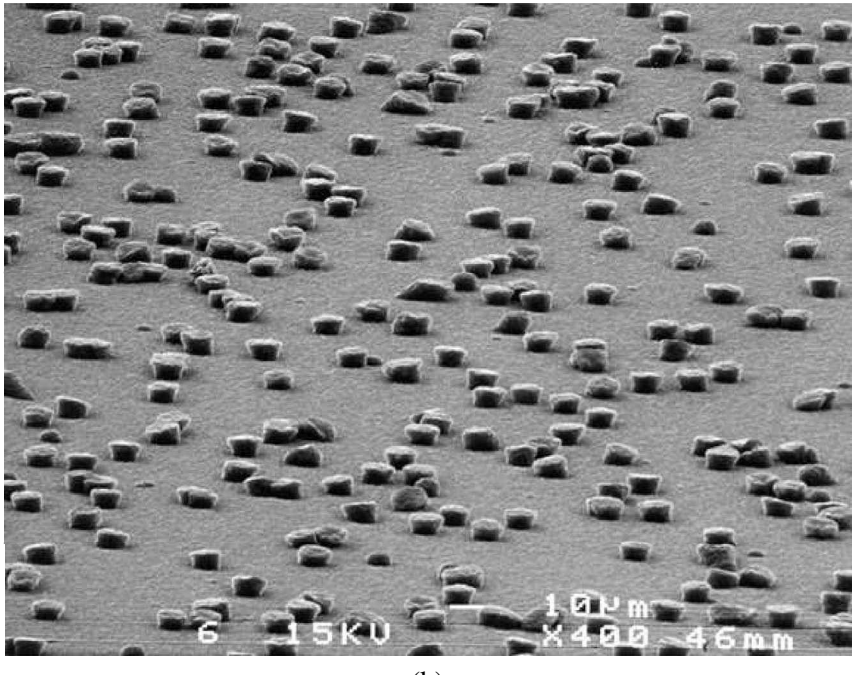

(b)

Figure 8. SEM micrographs of (a) polycarbonate membrane, and (b) molded silicone rubber hairs with about 6 μm diameter, 6 μm length, and 5×10^4 pores/cm^2 density.

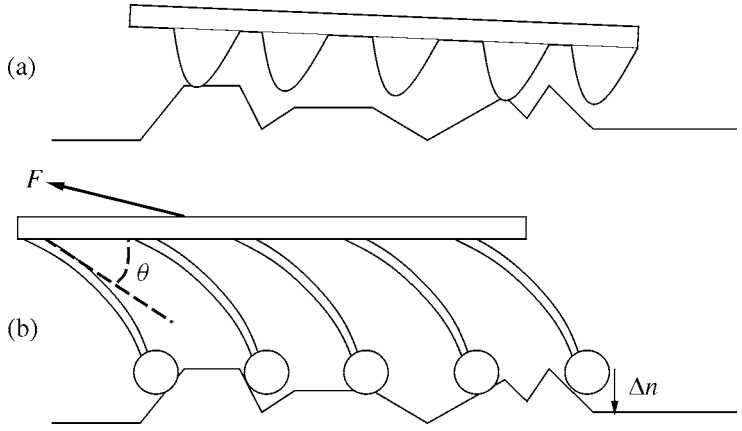

Figure 9. (a) Array of nanobumps. (b) Array of nanohairs.

3.1. Assumptions

We assume an end terminal on the setae which has a constant adhesion force of $F_o = 200$ nN normal to the surface, independent of hair orientation. (This could correspond to a spherical spatula at the end of setae.) We assume dry Coulomb friction with friction coefficient μ. Thus the spatula will slide if the tangential force at the spatula F_t is greater than $\mu(F_o - F_n)$, where F_n is the normal force component pulling the spatula off the surface. We assume quasi-static conditions (neglecting acceleration and dynamics), then $F_t \approx \mu(F_o - F_n)$ [13].

3.2. Non-matting condition

To prevent gecko hairs from sticking to each other, they must be spaced far enough apart and be stiff enough. We assume that the adhesion force between hairs is approximately equal to the adhesion force to the substrate. We also assume that the adhesion force is independent of stalk diameter, as the true contact radius at the terminal end of the stalk will be hard to control. Assume a point load at the end of a simple cantilever F_o, where F_o is the adhesion force on a spatula ($\approx$200 nN) as shown in Fig. 10.

First, we ensure the stalk is thick enough that the extension of the stalk does not need to be considered. Let stalk length and radius be l and r, respectively. Choose l, r such that the extensional stiffness k_x is much greater than the lateral stiffness k_y. For a cylindrical cantilever with modulus E_p, and moment of inertia $I = \pi r^4/4$, displacement Δ_y, the lateral stiffness k_y, and the stiffness along the beam axis k_x are computed as:

$$\Delta_y = \frac{F_y l^3}{3E_p I},$$

$$k_y = \frac{F_y}{\Delta_y} = \frac{3\pi r^4 E_p}{4l^3},$$

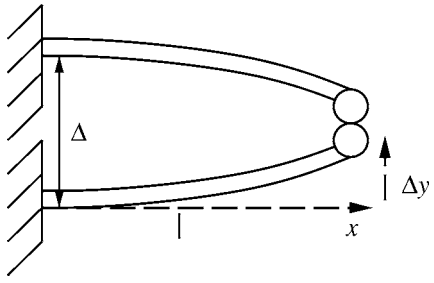

Figure 10. Single cantilever stalk with spatula at end.

$$k_x = \frac{\pi r^2 E_p}{l},$$
$$\frac{k_x}{k_y} = \frac{4l^2}{3r^2}. \tag{1}$$

To obtain a 100 : 1 ratio in stiffnesses, we use $l > 9r$.

Second, we must space the stalks far enough apart that the spatulae would prefer to stick to another surface rather than to each other. As shown in Fig. 10, the stalks are Δ apart, hence F_o must be less than $k_y \Delta/2$. Now given the adhesion force on a single spatula, the modulus of elasticity, the stalk length and radius, the minimum spacing Δ can be determined as:

$$\Delta \geqslant \frac{8F_o l^3}{3\pi r^4 E_p}. \tag{2}$$

Equation (2) only makes sense for $\Delta > 2r$, i.e. the spacing greater than the stalk diameter, for square lattice packing. This equation should also keep the stalks from buckling, since they are stiff enough to overcome the adhesion force.

Now we can calculate the adhesion pressure P_{adh} based on the force on each spatula and the area taken by each spatula stalk:

$$P_{adh} = \frac{F_o}{\Delta^2} = \frac{9\pi^2 E_p^2}{64F_o}\left(\frac{r^8}{l^6}\right). \tag{3}$$

Equation (3) offers several interesting observations:

1. Smaller F_o gives higher pressure. (With lower F_o, hairs can be smaller radius and closer.)
2. Stiffer stalks allow greater packing density.
3. Short, fat hairs give higher adhesion pressure. (However, short fat hairs are not desirable for adhering to rough surfaces.)

All of these observations depend on the assumption of avoiding sticking between hairs.

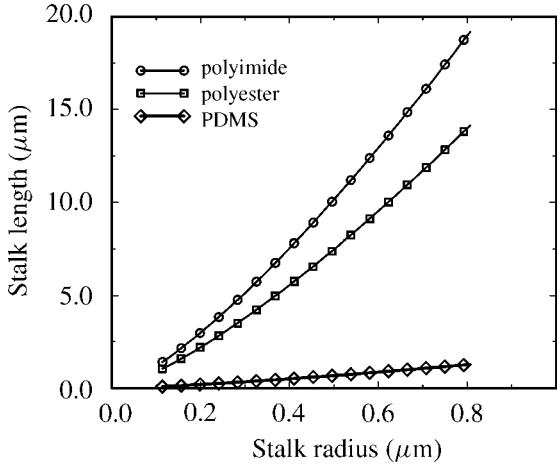

Figure 11. Maximum stalk lengths for different stalk radii and polymer materials (polyimide, polyester and PDMS) with no sticking between stalks (for adhesion pressure of 1 atmosphere).

Table 2.
Stalk parameters

Parameter	Polyimide	Polyester	PDMS
Young's modulus	2 GPa	850 MPa	600 kPa
adhesion force F_o	200 nN	200 nN	200 nN
l_{max} ($P_{adh} = 50$ kPa, $r_{max} = 1$ μm)	28 μm	20 μm	1.9 μm
l_{max} ($P_{adh} = 100$ kPa, $r_{max} = 0.7$ μm)	16 μm	12 μm	1.1 μm

For the last step, we need to fix a relationship between l and r to obtain a desired P_{adh}. We can find a maximum stalk radius for a square lattice simply from:

$$r_{max} = \frac{1}{2}\sqrt{\frac{F_o}{P_{adh}}}, \tag{4}$$

using minimum area of $4r^2$. Solving equation (3) for r, l, we obtain

$$\frac{r^4}{l^3} = \sqrt{\frac{64 P_{adh} F_o}{9\pi^2 E_p^2}} = \frac{8}{3\pi E_p}\sqrt{P_{adh} F_o} = l_o, \tag{5}$$

where l_o is a constant with units of length. Thus for a desired contact pressure, and hair length l, we must have

$$r = l_o^{1/4} l^{3/4} \quad \text{or} \quad l = l_o^{-1/3} r^{4/3}. \tag{6}$$

The parameters for polyimide, polyester and poly(dimethyl siloxane) (PDMS) rubber stalks are shown in Table 2. Note that the PDMS stalk is basically a bump, so

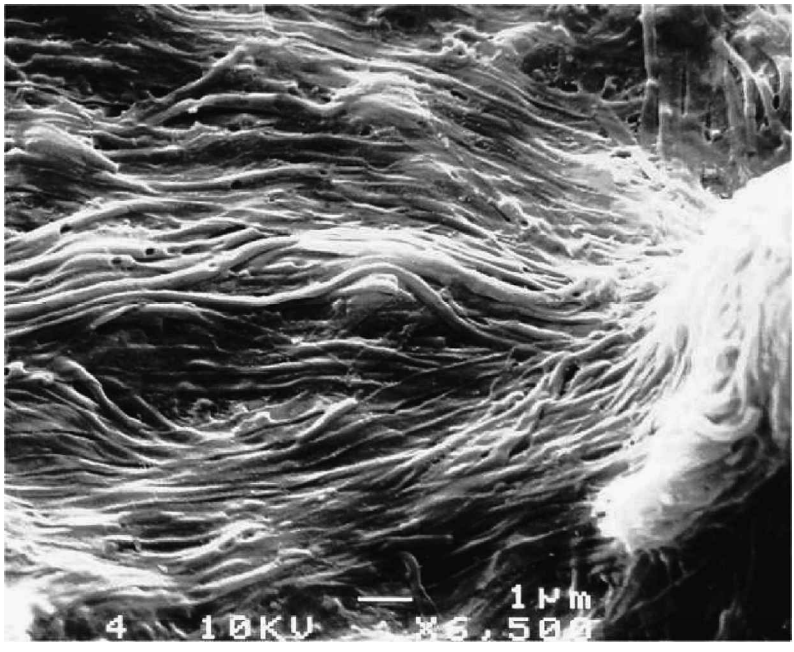

Figure 12. SEM micrograph of self-stuck very high aspect ratio (1 : 300) molded polyimide nano-hairs with 200 nm diameter and 60 μm length.

it will not provide any useful adhesion except to a perfectly planar surface. Figure 11 shows the maximum stalk length for a given stalk radius to avoid hairs sticking to each other. Packing density and sticking of hairs to each other limit maximum stalk lengths. It is interesting to note that with $r = 0.15$ μm stalk, the stalk length is only 1 μm. Hence a two-level structure of a longer, stiffer base stalk is required (setal structure) with fine terminal hairs (spatular hairs) to match rough surfaces.

In the molding experiments, a very high aspect ratio (1 : 300) polyimide (PI-2525, HD Microsystems Inc., Santa Clara, CA) nano-hairs with 200 nm diameter were fabricated. After molding, polyimide was cured, and the alumina membrane was etched away by HCl. The resulting nano-hairs are self-sticking bundles as displayed in Fig. 12. Due to the high density and very long (low stiffness) hairs, the non-matting condition was violated and the hairs stuck to each other.

3.3. Rough surface compatibility

Consider hairs contacting a rough surface as shown in Fig. 9b. During preload, the hairs may contact the surface at different heights, with a height variation Δn. The stiffness of the hair should be set such that the pull-off force $F_n = k_n \Delta n$ of a hair is less than the adhesion force F_o, otherwise hairs will pull off when the hairs are loaded. When contact is first made, there may be local sliding in the hair patch, which could also cause height variations Δn with rough surfaces.

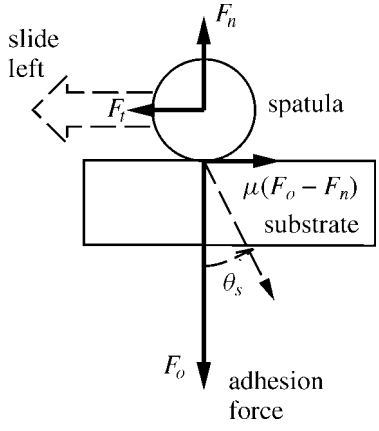

Figure 13. Friction, contact and adhesion forces acting on the spatula. An applied normal force $F_n < F_o$ attempts to pull the spatula off the surface. For quasi-static sliding, the tangential force F_t is balanced by the friction force $\mu(F_o - F_n)$.

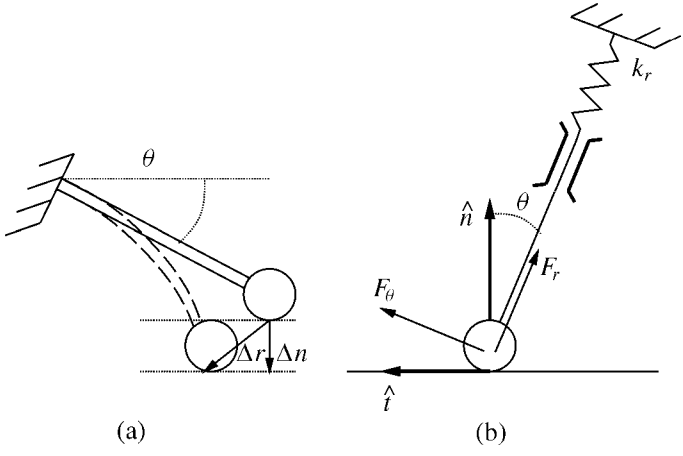

Figure 14. (a) Cantilever model for hair. (b) Forces on spatula from cantilever. F_r is the bending tension force pulling the spatula away from the surface. F_θ is the axial reaction force of the beam in the compression direction. The axial stiffness is assumed orders of magnitude stiffer than the bending stiffness.

Before modelling the setal hair, we review dry Coulomb friction with an added adhesion force as in Fig. 13. We assume that the limiting friction force is proportional to the normal force. We ignore any difference between sliding and static coefficients of friction. Note that as the normal force F_n increases, the tangential force F_t required to slide the spatula decreases. For sliding without acceleration (the quasi-static assumption), F_t exactly balances the friction force. At pull off, the friction force drops to zero, and hence $F_t \to 0$.

The setal hair can be modelled as a cantilever as shown in Fig. 14. Thus the setal hair has only one degree of freedom (bending motion Δr), with $\Delta\theta = 0$ [14].

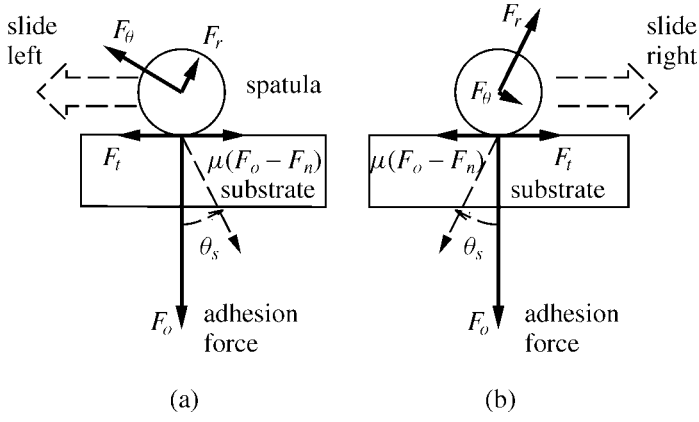

Figure 15. Contact friction force dependence on spatula sliding direction.

It is permissible for multiple hairs in a patch to slide on the surface. As long as contact is not broken, the hairs still contribute to net adhesion force. Consider a spatula contacting a surface as in Fig. 15. If the spatula slides, (under quasi-static conditions), the force on the spatula is on either edge of the contact friction cone (angle $\pm\theta_s$ from the surface normal, where $\theta_s = \tan^{-1}\mu$ is the friction angle).

Using these assumptions, we can now solve for the maximum normal displacement Δn when contact breaks. For quasi-static equilibrium the normal force F_n is equal to the pull-off force:

$$F_n = F_r \cos\theta + F_\theta \sin\theta = F_o. \tag{7}$$

At pull-off, since the friction force $\mu(F_o - F_n) = 0$,

$$F_t = -F_r \sin\theta + F_\theta \cos\theta = \mu(F_o - F_n) = 0. \tag{8}$$

For quasi-static equilibrium, equation (7) can be solved for F_θ:

$$F_\theta = F_r \tan\theta. \tag{9}$$

Thus the maximum radial force (due to the cantilever spring) at pull-off is:

$$F_r = F_o \cos\theta. \tag{10}$$

Now with bending stiffness k_r, $F_r = k_r \Delta r$, and $\Delta r = \Delta n / \cos\theta$ we obtain the maximum hair displacement before contact is broken:

$$\Delta n = \frac{F_o}{k_r} \cos^2\theta. \tag{11}$$

Equation (11) has some interesting implications. Clearly, if the hairs are normal to the surface, no surface roughness is allowed. If hairs are parallel to the surface, close to maximal compliance would be obtained, but there would not be room for many hairs. If there is significant contact friction, the friction allows a greater Δn, as would be expected since then the adhesion contact has both normal and tangential

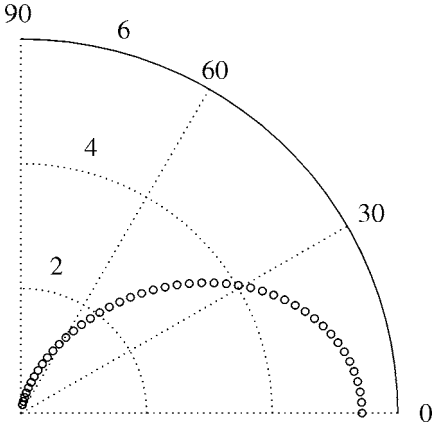

Figure 16. Maximum displacement Δn (2, 4, 6 μm) dependence on cantilever angle (for a polyimide stalk with $F_o = 100$ nN, $l = 10$ μm, $r = 0.25$ μm.) Long stalk which gives $\Delta n > 5$ μm violates matting condition.

components. The normal displacement Δn as a function of hair angle θ is shown in Fig. 16. It appears that $\theta = 30^\circ$ would give a reasonable compromise between surface roughness compatibility and spatula density.

3.4. A possible release mechanism

Consider again a hair at angle θ attached to a surface as in Fig. 17. Due to the compliance of the cantilever, the force in the $\hat{r}$ direction F_r is controlled by the displacement Δr. The axial force along the beam axis F_θ is a reaction force dependent on the applied force, adhesion force, friction coefficient and contact angle on the surface. For static contact, the net force $F_r\hat{r} + F_\theta\hat{\theta}$ is inside the friction cone. For quasi-static sliding, the force is at either the left or right edge of the friction cone, depending on sliding direction. By changing the sliding direction (pushing or pulling the cantilever parallel to the surface) the reaction force F_θ changes, hence the normal force may increase, leading to breaking of contact without explicitly pulling the spatula away from the surface.

For quasi-static sliding, the tangential force F_t exactly balances the sliding friction force $\mu(F_o - F_n)$. For the spatula sliding left as in Fig. 15a,

$$\begin{aligned} F_n &= F_r \cos\theta + F_\theta \sin\theta, \\ F_t &= -F_r \sin\theta + F_\theta \cos\theta = \mu(F_o - F_n). \end{aligned} \tag{12}$$

For the spatula sliding right as in Fig. 15b,

$$\begin{aligned} F_n &= F_r \cos\theta - F_\theta \sin\theta, \\ F_t &= F_r \sin\theta + F_\theta \cos\theta = \mu(F_o - F_n). \end{aligned} \tag{13}$$

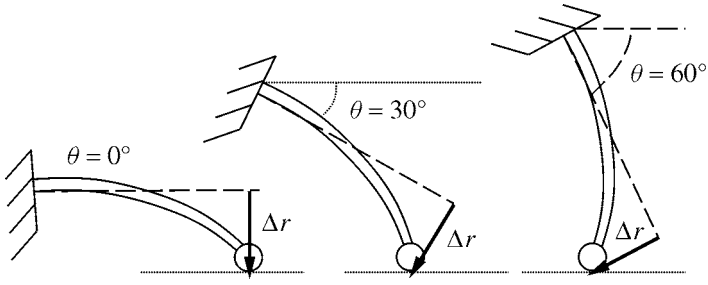

Figure 17. Cantilever hairs at $\theta = 0^\circ$, 30°, and 60°, with force $F_r = k_r \Delta r$. Small bending approximations are used.

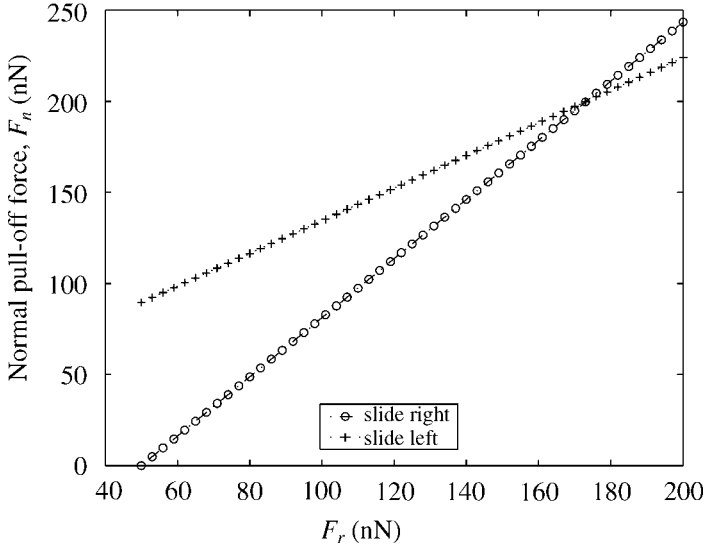

Figure 18. Predicted normal force on spatula for quasi-static sliding contact. Assumptions: hair is mounted at $\theta = 30^\circ$, $F_o = 200$ nN, $\mu = 0.5$. Spatula is more likely to release when sliding left due to higher normal (pull-off) force F_n than when sliding right.

Solving for the normal force F_n,

$$F_n = \frac{F_r \pm \mu F_o \sin\theta}{\cos\theta \pm \mu \sin\theta}, \tag{14}$$

where + and − correspond to sliding left and right, respectively.

The normal force equation, equation (14), when sliding to the right has several possible interesting implications. First, if $F_r < \mu F_o \sin\theta$, the contact will need to be pushed into the surface to slide to the right since $F_n < 0$. Perhaps this is helpful for preloading as spatulae will be encouraged to make contact. Second, the normal force is higher for sliding to the left, possibly increasing the tendency for the contact to pull-off (Fig. 18). (However, note that at pull-off, since the normal force exactly balances the adhesion force, the tangential force vanishes, hence friction should

have no effect at pull-off.) A third observation is that if the angle of the cantilever is changed while maintaining a constant F_r, the normal force becomes singular when $\tan\theta = 1/\mu$. It is interesting to speculate that the observed spatular/setal hair structure could act as a compound cantilever, thus changing the angle when pushing compared to pulling.

4. CONCLUSIONS

Nanomolding based synthetic gecko foot-hair fabrication methods and foot-hair adhesion and contact model for understanding the synthetic hair design issues are proposed. An AFM probe-based indented flat wax surface and self-organized alumina and polycarbonate nano-porous membranes were used as the master templates. The two methods resulted in nano-hairs with adhesion forces in the range of 180–300 nN and 60–100 nN, respectively, while the biological nano-hairs give adhesion force around 50–300 nN [1]. Thus, the generated sticking forces are similar, and we have shown that the adhesion forces are (1) relatively independent of material properties, (2) repeatable, (3) consistent with a standard adhesion model. Next, a gecko spatular hair model was proposed for showing the significance of the hair orientation, length, diameter, stiffness, and density. For adapting to rough surfaces, the following results were obtained: (1) Hairs can be stiff cantilevers to avoid matting. (2) For a non-matting cantilever model, hairs should be made of harder material, less sticky, fatter and shorter to get higher adhesion pressure. (3) For rough surfaces, hairs should be oblique to the surface, and compliant. Friction can improve adhesion effects. Changing the contact shear loading may provide a partial quick release mechanism. Hair attachment is quite robust to tangential displacement, but not to normal displacement. Oriented spatular stalk and stalk fabrication will be realized as a future work. Different versions of these synthetic adhesives will be used in future wall-climbing and surgical robot feet. Thus, high performance robots with low power consumption and high climbing and attachment/detachment maneuverability would become possible.

Acknowledgements

This work was supported by DARPA N66001-00-C-8047 and N66001-01-C-8072 from the Controlled Biological and Biomimetic Systems Program. The authors thank Kellar Autumn from Lewis and Clark College for measuring adhesion of the rubber hair array, and Murat Ozturk for assisting in membrane molding experiments.

REFERENCES

1. K. Autumn, Y. Liang, T. Hsieh, W. Zesch, W.-P. Chan, T. Kenny, R. Fearing and R. J. Full, *Nature* **405**, 681–685 (2000).

2. K. Autumn, M. Sitti, Y. A. Liang, A. M. Peattie, W. R. Hansen, S. Sponberg, T. Kenny, R. Fearing, J. N. Israelachvili and R. J. Full, *Proc. National Acad. Sci. (USA)* **99**, 12252–12256 (2002).
3. M. Sitti and R. S. Fearing, in: *Proc. of the IEEE Nanotechnology Conference*, Washington, DC, pp. 137–140 (2002).
4. M. Sitti and R. S. Fearing, in: *Proc. of the IEEE Robotics and Automation Conference*, Taiwan (2003) (to appear).
5. T. Dam and P. Pantano, *Rev. Sci. Instrum.* **70**, 3982–3986 (1999).
6. U. Drechsler, U. Durig, B. Gotsmann, W. Haberle, M. A. Lantz, H. E. Rothuizen, R. Stutz and G. K. Binnig, *IEEE Trans. on Nanotechnology* **1**, 39–55 (2002).
7. T. Borzenko, M. Tormen, V. Hock, J. Liu, G. Schmidt and L. W. Molenkamp, *Microelectronic Eng.* **57-58**, 389–396 (2001).
8. J. Vincent, *Structural Biomaterials*, rev. ed. Princeton University Press (1990).
9. J. Israelachvili, *Intermolecular and Surface Forces*, 2nd edn. Academic Press, London (1992).
10. M. Yu, T. Kowalewski and R. Ruoff, *Phys. Rev. Lett.* **86**, 87–90 (2000).
11. R. French, *J. Am. Ceram. Soc.* **83**, 2127–2146 (2000).
12. L. Li, V. Mangipudi, M. Tirrell and A. Pocius, in: *Fundamentals of Tribology and Bridging the Gap between the Macro- and Micro/Nanoscales*, B. Bhushan (Ed.), pp. 305–329. Kluwer, Dordrecht, The Netherlands (2001).
13. K. J. Salisbury and M. T. Mason, *Robot Hands and the Mechanics of Manipulation*. MIT Press, Cambridge, MA (1985).
14. R. S. Fearing, in: *Proc. of the IEEE Intl. Conf. on Robotics and Automation*, San Francisco, CA (1986).